processes

MDPI

Article

Detailed Analysis of the Cutoff Height in Composite Hard Rock Roofs Along Goaf Roadways

Jun Wu [1], Dongdong Bai [2], Yong Zhang [2], Qingwen Zhu [1,*], Peiyue Liu [2], Qingyu Chen [2] and Yuxuan Zhang [2]

[1] Shandong Key Laboratory of Civil Engineering Disaster Prevention and Mitigation, Shandong University of Science and Technology, Qingdao 266590, China; 13955372625@163.com
[2] Shandong Qiuji Coal Mine Limited Company, Dezhou 251106, China; 13791302510@163.com (D.B.); qjmkkjk@163.com (Y.Z.); luipeiyao@163.com (P.L.); 15965958138@163.com (Q.C.); 15244322730@163.com (Y.Z.)
* Correspondence: zhuqw@sdust.edu.cn

Abstract: To ensure lateral roadway retention in composite hard rock mining roofs, selecting a proper cutting height is crucial. If the cutting height is too low, the residual hard roof may experience secondary fractures under additional stress, which threatens roadway stability and safe mining production. Conversely, if the cutting height is too high, the overlying rock layers may bear uneven stress, increasing the risk of collapse. To conduct a detailed cutting height analysis for composite hard rock roof retention, the 12 1103 working face at the Qiuji Coal Mine was chosen as the research subject. Using the collapse characteristics of a goaf roof and the theory of composite beams, a lateral mechanical model of a goaf roof was constructed. By integrating the ultimate tensile stress theory and the Maxwell model, the optimal cutting height for a composite hard roof was derived. Using UDEC numerical simulation software, a model for lateral roadway retention was established to compare and analyze the roof collapse effects, vertical displacement, and vertical stress at different cutting heights. The results indicated that a cutting height of 7.8 m (with the bottom of the hole 0.48 m from the four gray layers) achieved the best cutting effect. Field engineering tests further validated the rationality of the calculated results. Using field surveys, the cutting height was adjusted from the original 9.35 m to 7.8 m for the 12 1103 working face. With a working face length of 946 m, this adjustment could save approximately 212,900 yuan in drilling construction costs and improve construction efficiency by 15%. This study provides a theoretical basis and practical reference for selecting cutting heights under similar geological conditions.

Keywords: composite rigid roof; mechanical model of cantilever beam cutting height; numerical simulation

check for updates

Academic Editor: Qingbang Meng

Received: 17 February 2025
Revised: 4 March 2025
Accepted: 10 March 2025
Published: 12 March 2025

Citation: Wu, J.; Bai, D.; Zhang, Y.; Zhu, Q.; Liu, P.; Chen, Q.; Zhang, Y. Detailed Analysis of the Cutoff Height in Composite Hard Rock Roofs Along Goaf Roadways. *Processes* **2025**, *13*, 838. https://doi.org/10.3390/pr13030838

Copyright: © 2025 by the authors. Licensee MDPI, Basel, Switzerland. This article is an open access article distributed under the terms and conditions of the Creative Commons Attribution (CC BY) license (https://creativecommons.org/licenses/by/4.0/).

1. Introduction

A hard roof is generally defined as rock strata that directly overlie a coal seam or are positioned immediately above the working face. This type of roof is characterized by its resistance to fracturing, susceptibility to pressure accumulation, high strength, robust integrity, and significant thickness [1–3]. In the Huanghebei coalfield of China, the No. 11 coal seam is overlain by a composite hard roof consisting of two layers of limestone interbedded with mudstone, with the floor facing potential threats from underlying hydrostatic pressure [4]. After the working face is advanced, the floor in the goaf becomes exposed, leading to changes in the stress state of the floor rock, which can cause upward bulging [5]. Owing to the considerable strength of the roof, it typically does not collapse immediately after a certain distance is mined, resulting in a phenomenon known as a "hanging roof". The

inability of the roof in the goaf to collapse in a timely manner can exacerbate floor heave, creating damage fracture zones within the floor rock, which may further trigger water inrush events [6,7]. Consequently, the deformation and failure of the floor are closely linked to the movement of the overlying rock. The timely and orderly collapse of the overburden above the goaf is a critical factor in ensuring safe production. The roof at the junction between the goaf and the roadway presents the greatest threat of collapse. To address this issue, we can draw on the top-cutting pressure relief technique proposed by academician He Manchao, which involves presplitting the roof at the advanced position of the working face to facilitate the orderly collapse of the roof in the goaf [8]. This method safely relieves pressure from the overlying strata and ensures the stability of the rock surrounding the roadway. The height and angle of the top cut are crucial parameters that influence the collapse behavior of the hard roof, with variations in the cutting height directly affecting both the conditions of roof collapse and the reloading effects on the floor in the goaf [9].

An appropriate top-cutting height not only ensures the smooth collapse of the roof but also enhances construction efficiency, reduces the quantity of explosives used, and minimizes costs. Su et al. established a stable structure and stress model for the surrounding rock in a reserved roadway to analyze the influence of the cut height and rock dilatation characteristics on the movement of the immediate roof [10]. Wang conducted research in a coal mine in the Qingyang western mining area and investigated the deformation and failure patterns of a rock mass during tunnel excavation, thereby exploring the mechanisms of roof failure and their control strategies [11]. Tian et al. constructed a mechanical model for hard roofs and determined that increasing the top-cutting height helps reduce stress on the coal wall of the roadway and minimizes roof subsidence [12]. Wang et al. employed mechanical modeling and numerical simulation techniques and reported that the adequacy of goaf filling and the thickness of the short cantilever beam are influenced primarily by the top-cutting height [13]. However, their models simplified geological heterogeneity, limiting practical application in complex strata. Their research also indicated that the selection of the top-cutting height and angle is not simply a maximization problem; rather, there exists an optimal range for these parameters. Liu et al. utilized UDEC simulations to capture fracture propagation under multi-scale geological variability [14]. Chen et al. proposed an AI-driven optimization framework for adaptive parameter selection [15]. Shi et al. utilized the PFC2D numerical simulation tool to reveal the logarithmic correlation between the top-cutting height and the pressure relief effect of the roof, as well as the nonlinear relationship between the cutting angle and the pressure relief effect [16]. Zhang et al. further validated these findings through field monitoring, emphasizing the necessity of site-specific calibration [17]. Yang et al., to ensure the successful implementation of top-cutting and reserved roadway techniques under conditions of thick coal seams and complex roof structures in the Guandi Coal Mine, established a mechanical model to analyze the factors affecting roof deformation and obtained reasonable top-cutting heights and angles through numerical simulations and field tests [18]. In contrast to prior studies (Table 1) focusing solely on static parameters, this work innovatively integrates dynamic roof behavior and real-time monitoring data, offering a hybrid framework for adaptive top-cutting design.

Table 1. Summary of methodologies for top-cutting parameter optimization.

Author	Method	Key Findings	Limitations	Applicability
Su et al. [10]	Stress-structure model	Cut height affects immediate roof movement	Ignored dynamic geological changes	Reserved roadways
Wang et al. [11]	Mechanical model	Top-cutting height affects goaf filling	Ignored dynamic loading	Homogeneous strata
Tian et al. [12]	Mechanical model	Increased height reduces coal wall stress	Assumed linear roof behavior	Hard roofs
Shi et al. [16]	PFC2D simulation	Log correlation: height vs. pressure relief	Limited to 2D analysis	Thin coal seams
Yang et al. [18]	Field tests + simulation	Optimal height for thick seams	Required extensive calibration	Guandi Mine conditions
Liu et al. [14]	UDEC simulation	Captures multi-scale fracture propagation	High computational cost	Deep, fractured roofs
Chen et al. [15]	AI optimization	Adaptive parameter selection	Requires large training data	High-gas, soft seams
Zhang et al. [17]	Field monitoring	Validates numerical models	Site-specific constraints	Thick coal seams

In summary, researchers have conducted numerous studies on the top-cutting height of hard roofs. However, most calculations for the top-cutting pressure relief height are based primarily on the theory of rock dilatation [19,20]. This theory posits that the rock fragments generated from the collapse of the roof can expand and fill the goaf within the range of the top-cutting height. Nonetheless, the dilatation characteristics of rock are influenced by various factors, including the physical and mechanical properties of the rock, the degree of fragmentation, and the fragment size. The complexity and variability of these factors can lead to inaccuracies in measuring and predicting the dilatation coefficient [21]. Therefore, the cutting height calculated via the theory of fragmentation often exhibits certain deviations. The rational selection of the cutting height is closely related to the safety of coal mine production. To determine the cutting height more accurately, this study focuses on the side roof of the goaf roadway and constructs a mechanical model of the roof rock beam, conducting a detailed analysis of the cutting height from a mechanical perspective.

This work uses the 12 1103 working face at the Qiuji Coal Mine as the engineering background to study the optimal cutting height for composite hard roofs. By constructing a mechanical model of the lateral roof in the goaf, this study comprehensively considers the fragmentation height of the gob material and the various conditions of the roof under loading from a mechanical perspective. The optimal cutting height for the composite hard roof is derived and calculated. Additionally, a model for lateral roadway retention is established via UDEC v7.0 numerical simulation software to further validate and optimize the theoretical results. Finally, the rationality of the cutting height is confirmed through monitoring results from roof anchor force gauges and roof separation meters in the field test sections, providing a theoretical basis and practical reference for selecting cutting heights under similar geological conditions.

2. Project Overview

The Qiuji Coal Mine is located in Dezhou city, Shandong Province, China. The current mining area is the 11th coal mining zone, with the 12 1103 working face situated in the 1211 mining zone, representing the third retrieval face in this area. To the north, it is adjacent to the auxiliary drainage roadway protecting the coal pillar, whereas to the south,

it borders the belt roadway of the 12th mining zone that protects another coal pillar. The eastern boundary is the 12 1104 working face, and to the west lies the 12 1102 working face, which has already been mined out, as shown in Figure 1b. The elevation of the 12 1103 working face ranges from −342 m to −448.7 m, corresponding to a surface elevation of +28.0 m to +29.8 m. The coal seam in the 12 1103 working face trends approximately east–west, with dip angles ranging from 4° to 12°, with an average of 7°. The conditions of the top and bottom plates of the coal seam in the 12 1103 working face are detailed in Table 2.

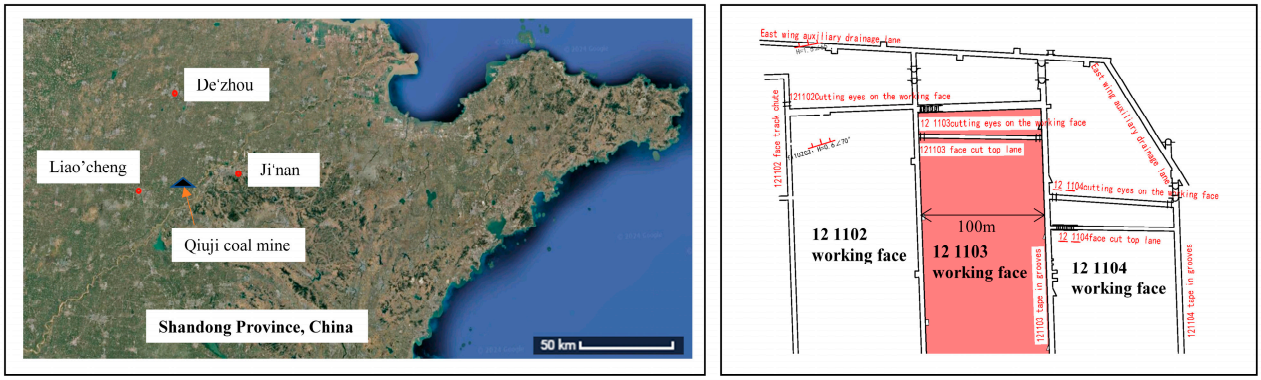

(a)Coal mine location **(b) General drawing of the working face**

Figure 1. Location and working face of the Qiuji Coal Mine.

Table 2. State of the coal seam top and bottom in the 12 1103 working face.

Roof and Floor Terminology	Rock Types	Thickness/(m)	Classification of Roof and Floor Strata	Mohs Hardness Scale *f*	Porosity (%)	Compressive Strength (MPa)
Direct Roof	Limestone	2.01	IV	13.557	6	135.57
Direct Floor	Mudstone	5.56	III	1.07	8.87	10.7

3. Theoretical Analysis of the Cutting Height of a Composite Hard Roof

For lateral roadway retention in composite hard roofs, the rational selection of the cutting height is a critical factor. Given that the roof consists of two layers of limestone interbedded with mudstone, the lower layer (five limestones) is particularly prone to collapse under the influence of cutting and the load from the overlying rock layers. The inherent low strength of the mudstone leads to its tendency to bend downward after cutting and mining operations, creating separation from the upper limestone layer. In contrast, the upper layer (four limestones) has greater strength and greater thickness, making it less likely to collapse after mining. Therefore, determining the cutting height for composite hard roofs relies primarily on the characteristics of the upper four limestone layers. If the cutting height is too small, incomplete fracture and collapse of the goaf roof rock may result, leaving gaps between the fallen rock and the roof. This inadequacy prevents the overlying rock layers from providing sufficient support, as shown in Figure 2a. Additionally, the residual hard roof may experience secondary fractures under additional stress, jeopardizing the stability of the roadway. Conversely, if the cutting height is excessively high, while it allows for complete collapse of the goaf roof (as illustrated in Figure 2b), it complicates the construction process, decreases drilling accuracy, and increases costs. Thus, an appropriate cutting height should comprehensively consider the effects of the roof's self-weight and the pressure from the overlying rock layers on roof collapse, as depicted in Figure 2c. Given this

context, further optimization and calculation of the cutting height are essential to increase construction efficiency and reduce production costs.

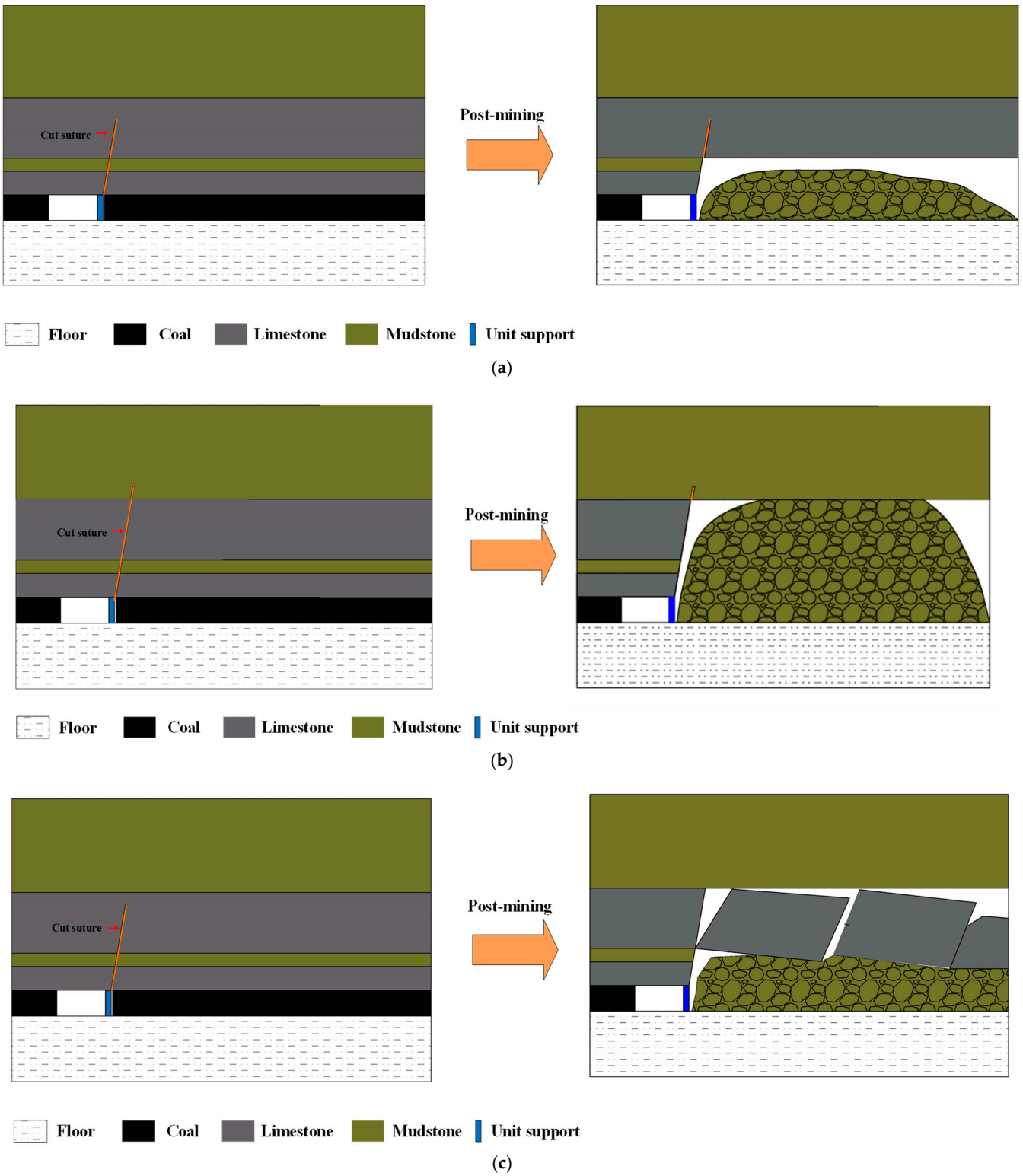

Figure 2. Roof collapse conditions of goafs under different paving heights. (**a**) The cutting height is insufficient; (**b**) the maximum cutting height is excessively high; (**c**) appropriate cutting height.

3.1. Calculation of the Overburden Load on the Roof Stratum

The original proposed cutting height on site is 9.35 m, with the cutting holes fully penetrating the upper four limestone layers and extending approximately 1 m into the

mudstone. Considering the relatively soft lithology of the mudstone overlying the basic roof and the self-weight of the limestone roof, the existing cutting height of 9.35 m is evidently excessive. Therefore, further optimization of the cutting height is necessary while maintaining the same support method. If the presplitting cut does not completely penetrate the upper four limestone layers, the lateral collapse condition of the overlying rock mass in the goaf area is illustrated in Figure 3a.

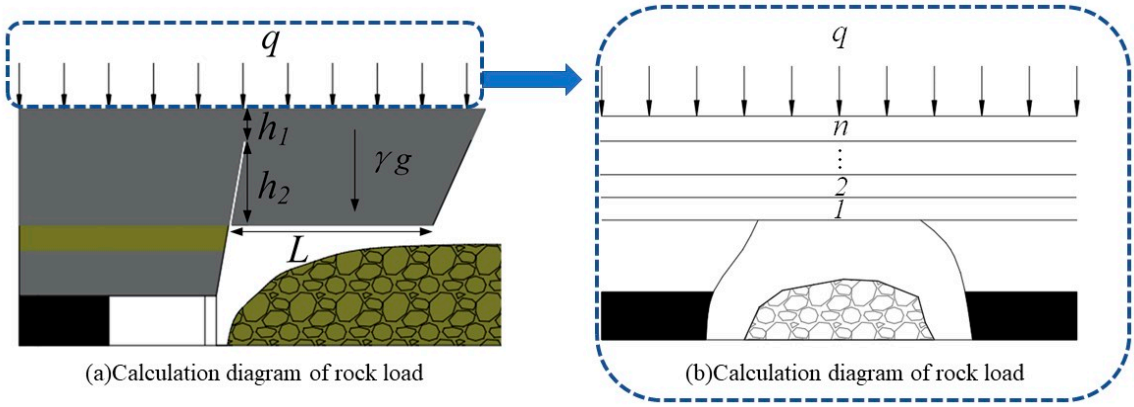

Figure 3. Caving model of the lateral overlying rock mass in the goaf of the working face.

On the basis of the actual conditions observed on site, after the working face retreated, the immediate roof of the limestone and mudstone collapsed rapidly. However, the gob material still fails to completely fill the goaf, resulting in the basic roof of the roadway not being supported by the gob. As a consequence, the roadway roof on the goaf side is unconstrained and can be treated as a cantilever beam. Assuming that the roadway roof is subjected only to its self-weight and pressure from the overlying strata, this can be modeled as a uniformly distributed load q. The length of the cantilever beam on the roadway side is L. The thickness of the four gray layers at the top-cutting portion is h_2, whereas the thickness of the remaining uncut limestone is h_1, with the relationship $h_1 + h_2 = 5.13$. To consider the load exerted by the overlying strata on the limestone of the basic roof, we can analyze this phenomenon via the principle of composite beams. The load calculation diagram for the composite beam rock layers is shown in Figure 3b. This analysis focuses on the load exerted by the n-th layer of rock over the upper four limestone layers of the basic roof [22]. To conduct this analysis, consider the following factors:

$$(q_n)_1 = \frac{E_1 h_1^3 (\gamma_1 h_1 + \gamma_2 h_2 + \cdots + \gamma_n h_n)}{E_1 h_1^3 + E_2 h_2^3 + \cdots + E_n h_n^3} \quad (1)$$

In the load analysis, E is the elastic modulus of the rock strata (in MPa). $h_1, h_2 \ldots h_n$ are the thicknesses of each layer of rock (in meters). $\gamma_1, \ldots \gamma_n$ are the unit weights of each layer of rock (in kN/m^3).

By substituting the parameters from Table 3 into the equation, we find that $(q_2)_1 < q_1$. Therefore, the self-weight of the basic roof rock strata accounts for the entire load experienced by the limestone at this moment. Consequently, the load exerted by the overlying rock layers on the basic roof can be considered negligible.

Table 3. Calculation parameters of the rock load.

Rock Strata	Lithology	Volume Force γ_i/(kN/m^3)	Layer Thickness h_i/(m)	Elastic Modulus E_i/(MPa)
1	Limestone	26	5.13	1.3×10^4
2	Mudstone	22.5	7.97	1.1×10^4
3	Siltstone	25.5	5.0	1.9×10^4
4	Silty Mudstone	21.5	2.01	1.5×10^4

3.2. Derivation of the Cutting Height Calculation Formula

To simplify the analysis of the cantilever beam in the goaf area and consider the presence of fallen gob material, the calculation model can be divided into two scenarios on the basis of the vertical displacement δ at the free end of the cantilever beam, as illustrated in Figure 4a,b.

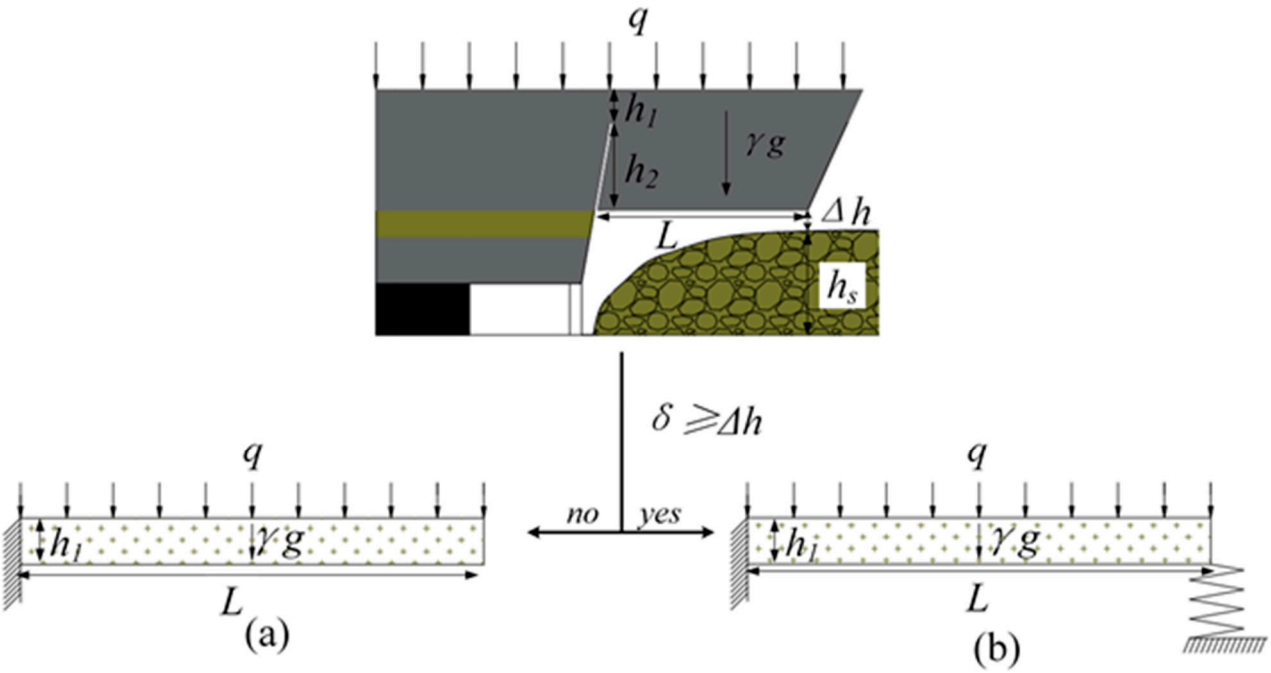

Figure 4. Lateral roof mechanical model of the goaf in the working face. (**a**) $\delta \geq \Delta h$ Cantilever beam; (**b**) $\delta < \Delta h$. A beam with one end fixed and one end simply supported.

Direct top caving rock fragments fill the goaf, and the height of the gob material h_s is the sum of the heights of the fragmented caved rock layers after collapse [23]:

$$h_s = \sum_{i}^{n} K_i z_i \tag{2}$$

where K_i is the elastic modulus of the rock layer, in MPa, and z_1, $z_2 \ldots z_n$ are the thicknesses of the collapsed roof rock layers.

Owing to coal seam extraction, the height of the goaf is greater than the thickness of the caved gob material. As a result, the free end of the lateral cantilever beam in the goaf experiences vertical displacement under the effects of the overlying rock layer load q and its self-weight load γg. The maximum vertical displacement is denoted as δ:

$$\delta = \frac{(q + \gamma g)L^4}{8EI} \tag{3}$$

The height difference Δh between the free end of the direct top caving roof and the fragmented gob material in the goaf is given by the following:

$$\Delta h = H - h_s \tag{4}$$

In the formula, H represents the sum of the coal seam height and the height of the caved rock layers.

If $\delta < \Delta h$, the roof behaves as a cantilever beam structure under loading until failure, as shown in Figure 4a. If $\delta \geq \Delta h$, the cantilever beam of the roof contacts the gob material under load, transforming into a beam with one end fixed and the other end supported elastically, as illustrated in Figure 4b.

(1) When $\delta < \Delta h$, according to structural mechanics, the maximum bending moment M and tensile stress $\sigma_{\max}$ occur at the free end (the side of the roadway). They are expressed as:

$$\begin{cases} M = \frac{1}{2} q_{total} L^2 \\ \sigma_{\max} = \frac{M}{W} \end{cases} \tag{5}$$

In these equations, the section modulus $W = hL^2/6$, where q_{total} is the sum of the overburden load and the self-weight load. $\sigma_{\max}$ is defined as the limit tensile strength of the roof limestone.

In this context, failure of the cantilever beam occurs when the tensile stress limit of the fixed end is reached. To calculate the cutting height, it is essential to consider the ultimate tensile strength at the fixed end.

$$\sigma_{\max} \leq [\sigma_t] \tag{6}$$

(2) When $\delta \geq \Delta h$, under loading, the free end of the original cantilever beam contacts the gob material. Owing to the support from the gob material at the free end, the beam transforms into a beam with one end fixed and the other simply supported. The support from the fragmented gob material in the goaf can be simplified to a spring support, where the spring stiffness k represents the compressive strength of the fragmented gob material. The deformation of the spring h(t) is a function of time [24].

Owing to the nonconstant support provided by the gob material at the right end of the goaf, it is not feasible to analyze the cutting height via classic structural mechanics. Under the action of loads, the settlement of the roof beam in the goaf will eventually stabilize, which can be used to calculate the optimal cutting height.

To study the settlement of the free end of the roof beam, the intact basic roof can be modeled as a viscoelastic beam, with material properties that conform to the Maxwell model. The constitutive equation for this model is given by [25]:

$$\frac{\partial \varepsilon}{\partial t} = \left(\frac{1}{E} \frac{\partial \sigma}{\partial t} + \frac{\sigma}{\eta} \right) \tag{7}$$

The relationship between the linear strain ε of the roof beam when it is bending and the settlement $W(x,t)$ can be expressed as follows:

$$\varepsilon = y \frac{\partial W(x,t)}{\partial x^2} \tag{8}$$

Substituting ε and $W(x,t) = \partial w(x,t)/\partial t$ into Equation (7), we obtain the following:

$$y \frac{W(x,t)}{\partial x^2} = \left(\frac{1}{E} \frac{\partial \sigma}{\partial t} + \frac{\sigma}{\eta} \right) \tag{9}$$

By multiplying both sides of the equation by ydA and integrating over the cross-section, we obtain the following:

$$\frac{\partial W(x,t)}{\partial x^2}\int_A y^2 dA = \left(\frac{1}{E}\frac{\partial \sigma}{\partial t}\int_A y^2 dA + \frac{\sigma}{\eta}\int_A y^2 dA\right) \tag{10}$$

The moment of inertia I_1 of the roof beam and the bending moment $M(x,t)$ are given by the following:

$$\begin{cases} I_1 = \int_A y^2 dA \\ M(x,t) = \int_A \sigma_y dA \end{cases} \tag{11}$$

Substituting Equation (11) into Equation (10), we obtain the following:

$$I_1\frac{\partial W(x,t)}{\partial x^2} = \left(\frac{1}{E}\frac{\partial M(x,t)}{\partial x^2} + \frac{\partial M(x,t)}{\eta}\right) \tag{12}$$

From the structural model in Figure 4b, the deflection equation of the roof is as follows:

$$W(x,t) = \frac{1}{EI}\left[\begin{array}{l} \frac{K\Delta h(t)xL^2}{3} - \frac{q_{total}L^3x}{8} + \frac{k\Delta h(t)L^2(L-x)}{2} - \frac{K\Delta h(t)(L-x)^3}{6} \\ -\frac{q_{total}L^3(L-x)}{6} + \frac{q_{total}(L-x)^4}{24} - \frac{K\Delta h(t)L^3}{3} \end{array}\right] \tag{13}$$

When $t = 0$ and $x = 0$ or L, the settlement $W(x,t) = 0$, satisfying the initial conditions. Taking the partial derivatives of Equation (13) with respect to t and x, we obtain the following:

$$\frac{\partial W(x,t)}{\partial x^2} = \frac{k}{EI_1}(L-x)\frac{\partial \Delta h(t)}{\partial t} \tag{14}$$

The bending moment equation for the roof beam is given by the following:

$$M(x,t) = k\Delta h(t)(L-x) - q_{total}(L-\mathrm{x})^2/2 \tag{15}$$

By taking the partial derivative of the bending moment with respect to t and substituting it along with Equation (14) into the deflection equation while setting $x = 0$, we can establish the differential equation $\Delta h(t)$, which contains only the following:

$$\frac{\partial \Delta h(t)}{\partial t} + \frac{E}{2\eta}\Delta h(t) = \frac{ELq_{total}}{4k\eta} \tag{16}$$

Solving the above first-order linear differential equation, the solution is as follows:

$$\Delta h(t) = q_{total}L/2k + Ce^{-E^t/2\eta} \tag{17}$$

Using the initial condition to determine the integration constant, when $t = 0$ and $\Delta h(t) = 0$, we find $C = -q_{total}L/2k$. Substituting this back into the equation, we can derive the dynamic equation for the side settlement of the roof's mining area:

$$\Delta h(t) = \frac{q_{total}L}{2k}\left(1 - e^{-E^t/2\eta}\right) \tag{18}$$

Differentiating with respect to time t, we obtain the settlement velocity equation:

$$\frac{\partial \Delta h(t)}{\partial t} = \frac{ELq_{total}}{4k\eta}e^{-\frac{E^t}{2\eta}} \tag{19}$$

When $t = 0$, we have $\Delta h(t) = 0$ and $\partial \Delta h(t)/\partial t = Eq_{total}L/4k\eta$. As $t \to \infty$, $\Delta h(t)$ approaches $\Delta h(t) \to q_{total}L/2k$, and the settlement velocity tends to $\partial h(t)/\partial t \to 0$.

Therefore, under the action of the load, the settlement of the roof beam in the mined-out area gradually approaches a stable value.

When $t = T$, the settlement amount of the roof reaches a stable state and is given by the following:

$$\Delta h(T) = h - (K_p - 1)h_1 \tag{20}$$

where h represents the thickness of the coal seam; K_p denotes the average swelling coefficient of the broken rock in the mined-out area; and h_1 is the thickness of the roof.

By substituting $\Delta h(T)$ into Equation (18), we can derive the calculation formula for the relationship between the time it takes for the rock beam to reach a stable state and the beam thickness:

$$h_1 = \frac{1}{K_p - 1}\left[M - \frac{q_{total}L}{2k}\left(1 - \frac{1}{e^{\frac{ET}{2\eta}}}\right)\right] \tag{21}$$

In this equation, E is the elastic modulus of the basic roof. T represents the time required for the rock beam to reach a stable state, which is calculated on the basis of the minimum required top distance and the extraction speed. η is the shear modulus of the basic roof. L denotes the lateral cantilever length of the mined-out area. M represents the thickness of the coal seam. K_p is the average swelling coefficient of the rock layer. h_1 represents the thickness of the roof after top cutting. k denotes the compressive strength of the rubble.

By substituting the coefficients from the Qiuji Coal Mine 12 1103 working face into Formulas (2)–(4), we find that $\delta < \Delta h$. Therefore, the roof remains a cantilever beam structure under the load until failure. The tensile strength of the roof limestone $[\sigma_t]$ is 3.16 MPa. Considering that there is a collapse phenomenon in the rock layers beneath the four limestone layers, we reduce the self-weight load of the limestone that has been cut by a reduction factor of 0.75. Thus, the uniformly distributed load on the cantilever beam is given by $q_{total} = \gamma h_1 + 0.75\gamma h_2$. Substituting the above coefficients into Equation (22) and solving together gives the relationship between the cutting height and the lateral cantilever length of the mined-out area:

$$\sigma_{\max} = \frac{3[\gamma h + 0.75\gamma(5.13 - h)]L}{h^2} \le [\sigma_t] \tag{22}$$

In the field, the observational data for the maximum cantilever length in the noncollapse area of the 11 completed coal working faces are summarized in Table 4. Taking the average, we find that the maximum lateral cantilever length of L in the mined-out area is 4.5 m. Substituting this value into Equation (4) yields $h_{\max} = 0.48$ m; thus, the cutting height is 7.8 m.

Table 4. Maximum overhang length of the noncaving area behind the coal face support in Layer 11.

Name of the Working Face	Maximum Lateral Cantilever Length in Uncaved Area Behind Frame/(m)
Working Face 11 1107	4.7
Working Face 11 1108	4.4
Working Face 12 1101	4.6
Working Face 12 1103	4.3

4. Numerical Simulation Verification

4.1. Numerical Model and Parameters

On the basis of the engineering background of the Qiuji Coal Mine 12 1103 working face, we utilized the discrete element simulation software UDEC 7.0 to establish coal mining models under different cutting heights. UDEC was selected for this study due to its superior capability in modeling discontinuous media and simulating the progressive failure processes in jointed rock masses, which is particularly relevant for understanding roof subsidence behavior in underground mining. While other numerical approaches, such as finite element methods (FEMs) and alternative constitutive models like Hardening Soil could be considered, the discrete element method better captures the blocky nature of the stratified roof structure, and the large displacements associated with mining-induced cave-in scenarios. The model dimensions are 200 m (length) × 50 m (height), with a boundary of 45 m on each side. The numerical model contained 466,139 elements and 471,189 nodes for a cutting height of 0 m; 471,399 elements and 471,469 nodes for a cutting height of 7 m; 471,707 elements and 471,697 nodes for a cutting height of 7.5 m; 472,747 elements and 472,537 nodes for a cutting height of 7.8 m; 473,055 elements and 472,845 nodes for a cutting height of 8 m; 474,209 elements and 474,044 nodes for a cutting height of 8.2 m; 474,517 elements and 474,352 nodes for a cutting height of 8.4 m; and 475,203 elements and 475,090 nodes for a cutting height of 8.5 m. The lateral and basal boundaries were prescribed fixed displacement constraints, while a vertical compressive stress of 11.7 MPa was imposed on the upper boundary to replicate in situ geostatic stresses. The bottom and sides of the model are constrained in displacement, and the Mohr–Coulomb yield criterion is selected, as illustrated in Figure 5. The Mohr–Coulomb constitutive model was adopted due to its well-established applicability in geotechnical engineering, particularly for coal measure rocks, and its ability to effectively represent the shear failure mechanism predominant in roof collapse. Although more advanced constitutive models such as Hardening Soil could potentially provide more refined stress–strain relationships incorporating strain hardening behavior, the Mohr–Coulomb model offers a reasonable compromise between computational efficiency and accuracy for the specific objectives of this comparative study. A comparative analysis is performed to evaluate roof subsidence under different cutting heights. The selected physical and mechanical parameters of the main rock layers are presented in Table 5.

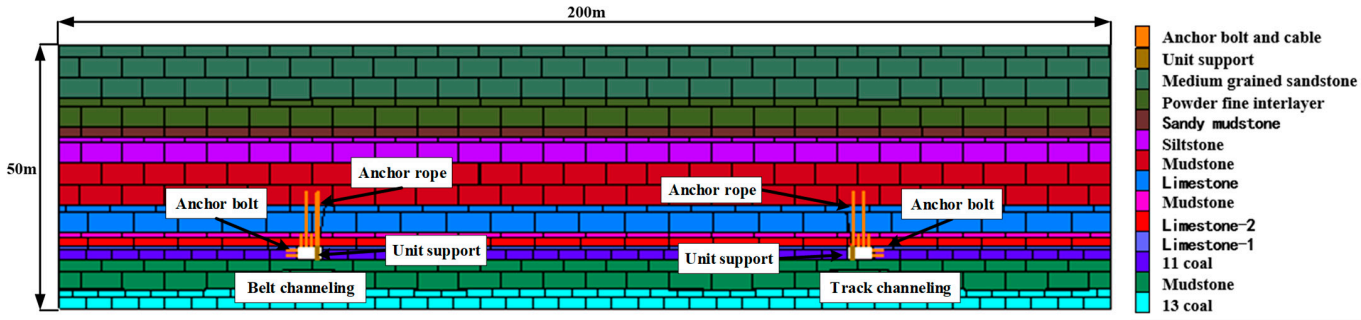

Figure 5. Numerical calculation model for different cutting heights.

Table 5. Physical and mechanical parameters of the main rock formations.

Name	Density (kg/m^3)	Normal Stiffness (GPa)	Shear Stiffness (GPa)	Cohesive Force (MPa)	Friction Angle (°)	Tensile Strength (MPa)
Silt-Clay Interbedding	2540	10.23	3.43	2.96	35	3.26
Silty Mudstone	2240	3.27	1.43	1.52	26	1.28
Siltstone	2550	7.55	2.94	2.34	35	3.47
Mudstone	2250	4.59	1.79	1.47	25	1.54
Limestone	2600	16.84	8.12	3.02	35	3.16
Mudstone	2250	4.59	1.79	1.47	25	1.54
Limestone	2600	16.84	8.12	3.02	35	3.16
Type 11 Coal	1420	2.45	0.91	1.50	28	1.14
Mudstone	2250	4.59	1.79	1.47	25	1.54
Type 13 Coal	1420	2.45	0.91	1.50	28	1.14

4.2. Numerical Analysis of Different Cutting Heights

Using the theoretical cutting height of 7.8 m as a baseline and considering the geological conditions of the Qiuji Coal Mine 12 1103 working face, we designed eight different cutting heights for simulation experiments through the method of controlling variables: 0 m (reference group without cutting), 7 m, 7.5 m, 7.8 m, 8 m, 8.2 m, 8.4 m, and 8.5 m. To simplify the model construction, the cutting angle in the models is uniformly set at the optimal angle of 10°, which has been determined through both theoretical calculations and field practices.

(1) Analysis of roof collapse conditions

Figure 6 shows the roof collapse conditions in the mined-out area under eight different cutting heights: 0 m (no cutting), 7 m, 7.5 m, 7.8 m, 8 m, 8.2 m, 8.4 m, and 8.5 m. When no cutting operation is implemented (i.e., the cutting height is 0 m), as shown in Figure 6a, the roof near the tunnel side tends to form a cantilever structure, exerting significant pressure on the support structure of the 12 1103 working face, leading to considerable deformation and substantial roof subsidence. Additionally, owing to the failure of the roof to collapse in a timely manner to relieve pressure on the floor, there is a noticeable uplift in the mined-out area. At cutting heights of 7 m and 7.5 m, as depicted in Figure 6b,c, the direct roof of the five gray layers and mudstone can bend and collapse along the cutting seam. However, the collapse effect of the basic roof of the four gray layers is not satisfactory, resulting in deformation of the roadway support structure, with significant roof subsidence and uplift in the mined-out area. The pressure relief effect at these cutting heights is not optimal. At a cutting height of 7.8 m, as shown in Figure 6d, the cutting height is 0.48 m below the top of the basic roof's four gray layers. Both the direct roof and the basic roof bend and collapse downward along the cutting seam. The roadway support structure shows minimal deformation, and the overall deformation of the tunnel is relatively slight, leading to significant improvement in the uplift of the mined-out area. For cutting heights greater than 7.8 m, as illustrated in Figure 6e–h, the deformation of the roadway tends to stabilize.

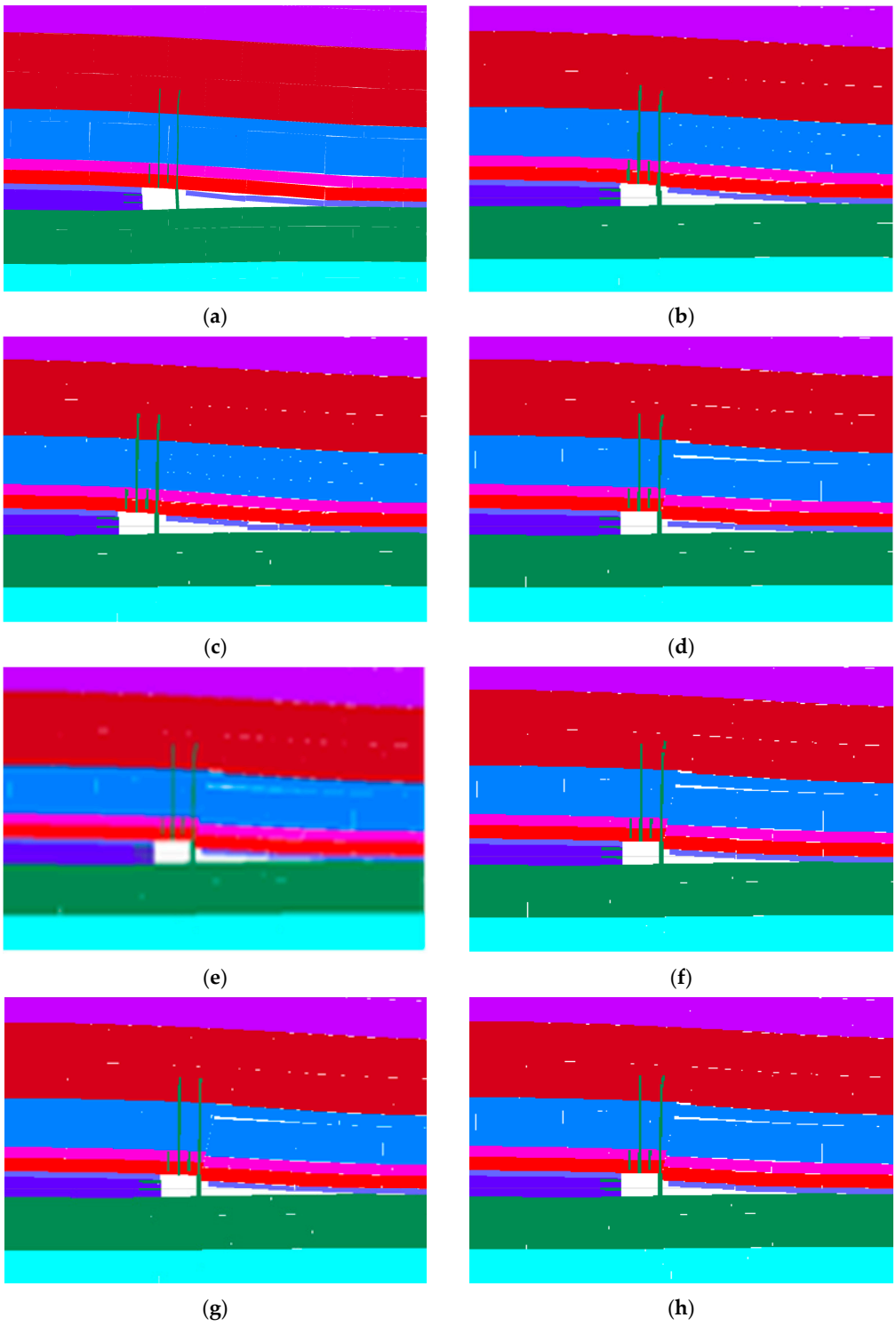

Figure 6. Roof caving at different cutting heights. (**a**) Cutoff Height of 0 m; (**b**) Cutoff Height of 7 m; (**c**) Cutoff Height of 7.5 m; (**d**) Cutoff Height of 7.8 m; (**e**) Cutoff Height of 8 m; (**f**) Cutoff Height of 8.2 m; (**g**) Cutoff Height of 8.4 m; (**h**) Cutoff Height of 8.5 m.

(2) Analysis of vertical displacement in the pillar roadway roof

An analysis of the vertical displacement cloud maps in Figure 7a–h reveals that the maximum subsidence of the roof occurs on the side of the mined-out area of the roadway and decreases toward the solid coal side. Specifically, the green regions (>800 mm) in Figure 7a indicate the highest displacement near the mined-out boundary, transitioning to yellow (200–600 mm) in the roadway center and blue (<200 mm) on the solid coal side

(see colorbar in Figure 7). The vertical displacement of the roadway roof varies with the cutting height, as shown in Figure 8. In the case of the no-cutting operation, the maximum vertical displacement of the roof on the side of the mined-out area reaches 699 mm. When the cutting height is set to 7–7.5 m (Figure 7c,d), the vertical displacements on the solid coal side, the center of the roadway, and near the mined-out area decrease by 22.9%, 3.6%, and 7.8%, respectively, compared with those in the no-cutting scenario. At a cutting height of 7.8 m, the vertical displacement reaches its minimum value, with reductions of 24.9%, 26.9%, and 30.8% for the solid coal side, the center of the roadway, and near the mined-out area, respectively, compared with the no-cutting scenario. For cutting heights of 8–8.5 m, no significant changes in vertical displacement are observed.

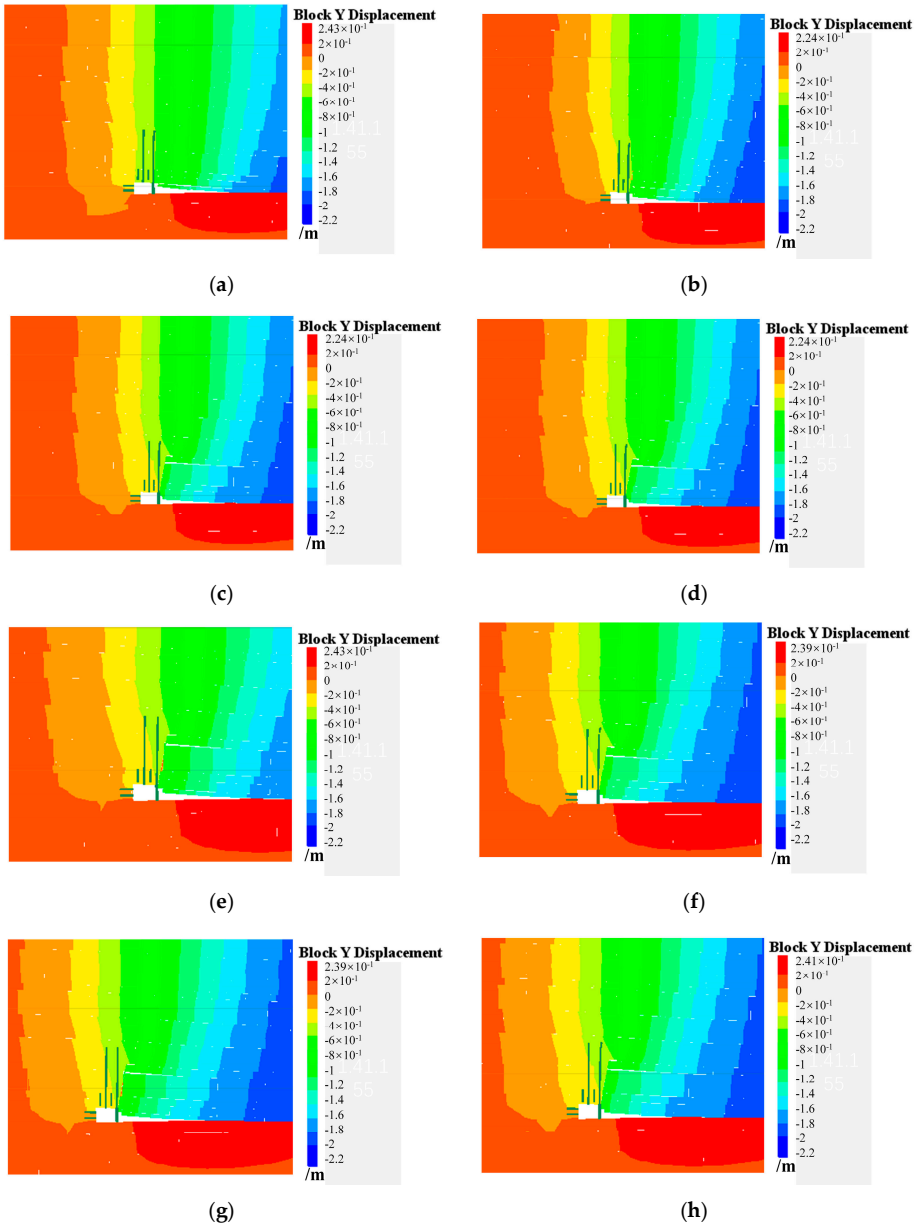

Figure 7. Vertical displacement cloud image of roadway retention at different cutting heights. (**a**) Cutoff Height of 0 m; (**b**) Cutoff Height of 7 m; (**c**) Cutoff Height of 7.5 m; (**d**) Cutoff Height of 7.8 m; (**e**) Cutoff Height of 8 m; (**f**) Cutoff Height of 8.2 m; (**g**) Cutoff Height of 8.4 m; (**h**) Cutoff Height of 8.5 m.

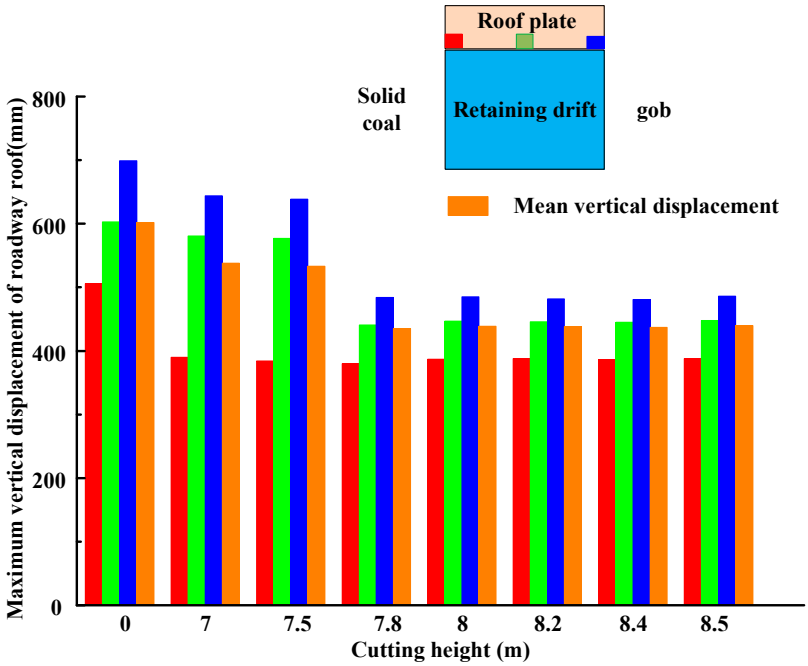

Figure 8. Column chart of the vertical displacement of the roof of the roadway with the height of the top cut.

(3) Analysis of the vertical stress in the pillar roadway roof

An analysis of the vertical stress cloud maps in Figure 9a–h reveals that the concentrated area of vertical stress on the roof of the roadway is located between the centerline of the tunnel and the solid coal side, decreasing toward the mined-out area. The stress hotspots (green, >28 MPa in Figure 9a) align with the uncut hard roof layers, while low-stress zones (orange, <10 MPa) dominate the mined-out side. The variation in the vertical stress in the roadway roof with increasing cutting height is shown in Figure 10. When no cutting operation is performed, the maximum vertical stress in the center of the roof reaches 28.1 MPa. At cutting heights of 7 m and 7.5 m, the vertical stress at the center of the roadway decreases by 90.7% and 90%, respectively, compared with that in the no-cutting scenario. Conversely, the vertical stress on the solid coal side increases by 18.9% and 21.4%, respectively. This observation, combined with the roof collapse conditions and vertical displacement cloud maps, indicates that the cutting heights of 7 m and 7.5 m did not effectively penetrate the four gray layers. The roof's self-weight and the overlying rock pressure were insufficient to cause the uncut portion to fracture, resulting in a redistribution of vertical stress during the roof collapse process. At a cutting height of 7.8 m, the vertical stress distribution returns to normal. For cutting heights of 8–8.5 m, the vertical stress distribution tends to stabilize.

In summary, a comparative analysis of roof collapse, vertical displacement, and vertical stress at different cutting heights indicates that at a cutting height of 7.8 m, both the vertical displacement and vertical stress of the roadway roof have reached optimal values. As the cutting height continues to increase, there is no significant change in vertical stress, and further enhancement of roadway stability shows no evident benefits. Additionally, increasing the cutting height increases the construction workload, wastes resources, and adversely affects production schedules.

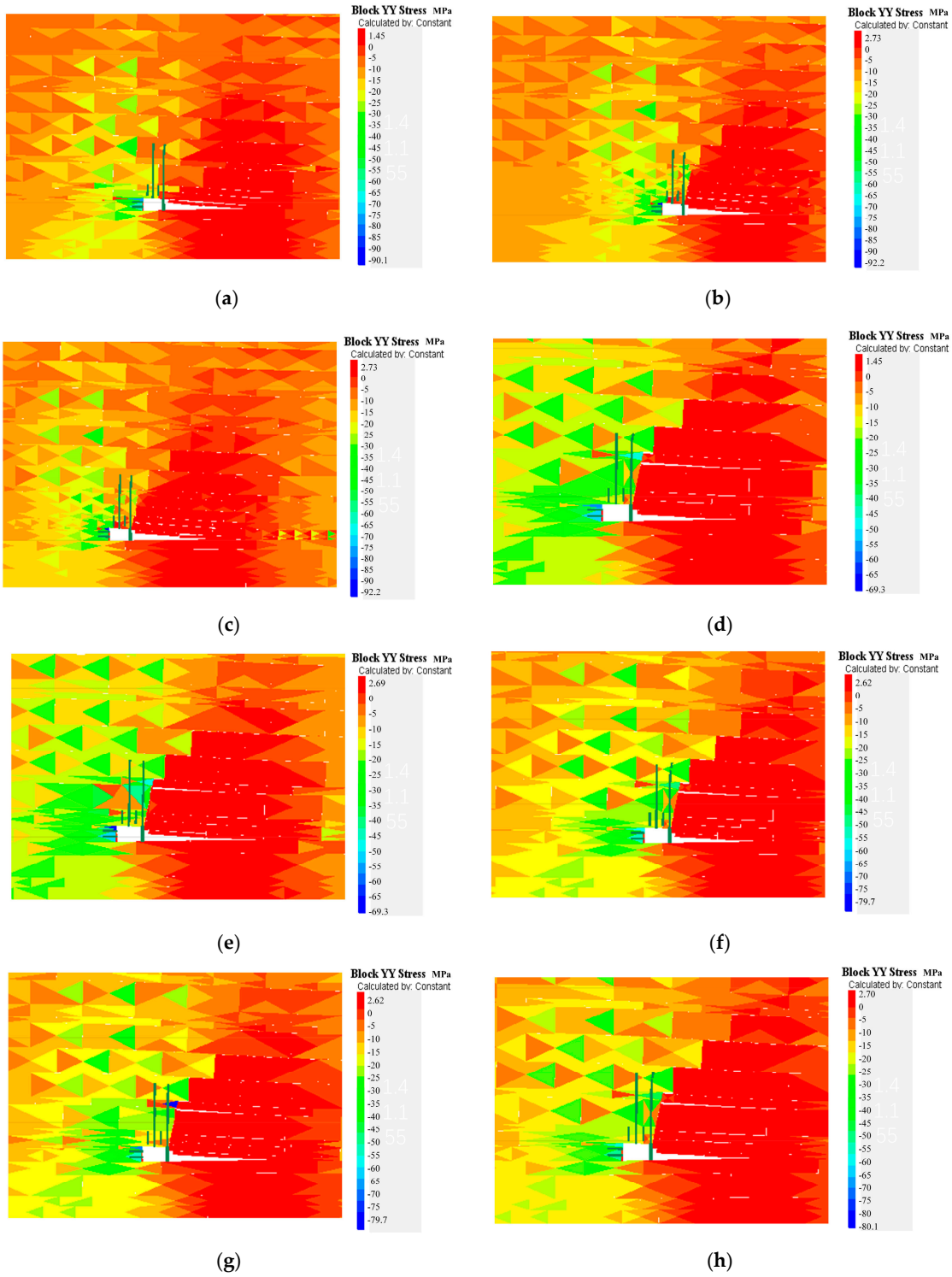

Figure 9. Vertical stress cloud image of roadway retention at different cutting heights. (**a**) Cutoff Height of 0 m; (**b**) Cutoff Height of 7 m; (**c**) Cutoff Height of 7.5 m; (**d**) Cutoff Height of 7.8 m; (**e**) Cutoff Height of 8 m; (**f**) Cutoff Height of 8.2 m; (**g**) Cutoff Height of 8.4 m; (**h**) Cutoff Height of 8.5 m.

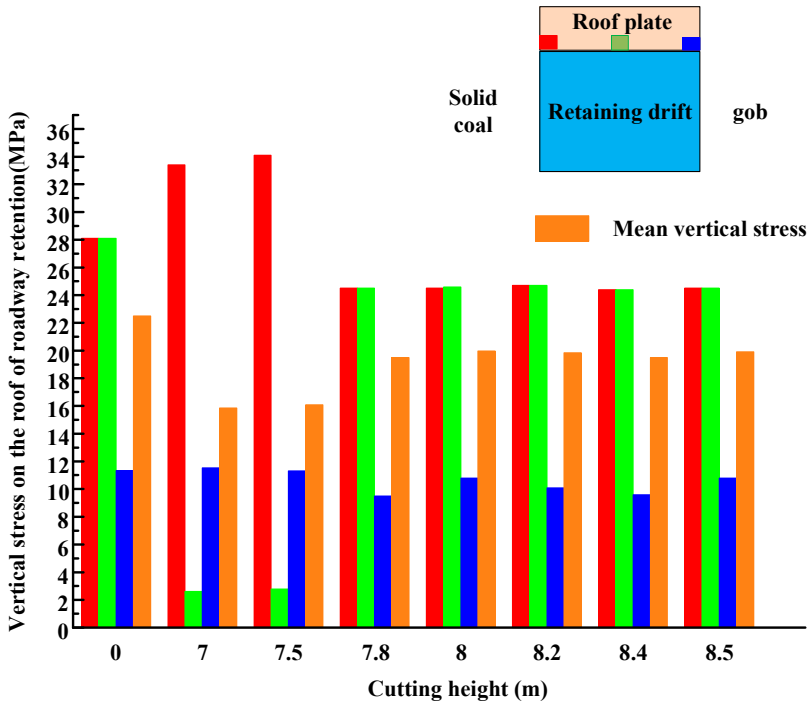

Figure 10. Column chart of the vertical stress of the roof of the roadway with the height of the top cut.

5. Field Testing

5.1. Implementation of Testing

To study the optimal cutting height of composite hard roofs under the condition of leaving roadways, experiments were conducted in specific sections of the 12 1103 working face at the Qiuji Coal Mine without affecting normal production. The experimental plan involved selecting two 30 m sections, starting 400 m from the cutting hole in the working face roadway, where drilling was performed at cutting heights of 7.8 m and 8 m, respectively. The remaining sections were drilled according to the original plan with a cutting height of 9.35 m. In all three sections, monitoring was carried out via anchor cable load cells and roof separation instruments to measure the roof conditions. The layout of the anchor cable load cells and roof separation instruments is illustrated in Figure 11.

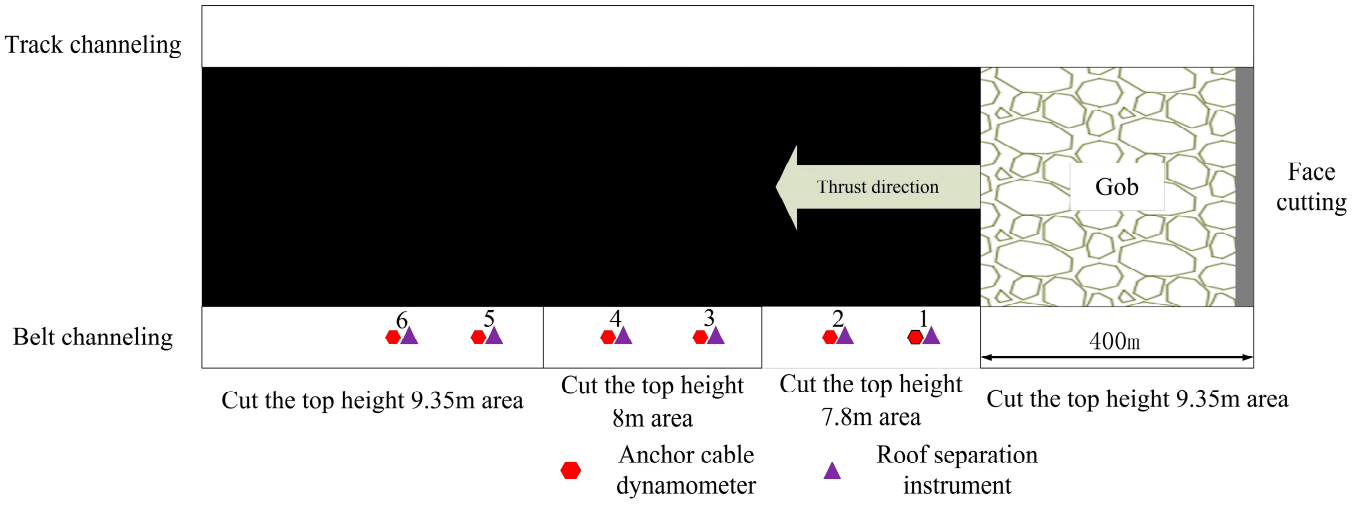

Figure 11. Distribution of the test section and monitoring instrument.

5.2. Roof Pressure Manipulation Patterns Before and After Roof Cutting

In the drilling experimental sections with cutting heights of 7.8 m and 8 m, as well as in the normal section, two sets of roof anchor cable load cells and roof separation instruments were arranged at advanced positions for monitoring and analysis. These instruments are numbered 1 to 6, and their layout is illustrated in Figure 10.

(1) The anchor cable load cells

The monitoring curves of the anchor cable load cells are shown in Figure 12. An analysis of these curves indicates that at cutting heights of 7.8 m, 8 m, and 9.35 m, the stress variation trends of the roadway roof anchor cables are similar. Once the roof pressure stabilizes, the stress measured by the anchor cable load cells approaches the initial pressure difference. Therefore, the optimal cutting height for the composite hard roof is determined to be 7.8 m, which is more economical and reasonable than the original plan.

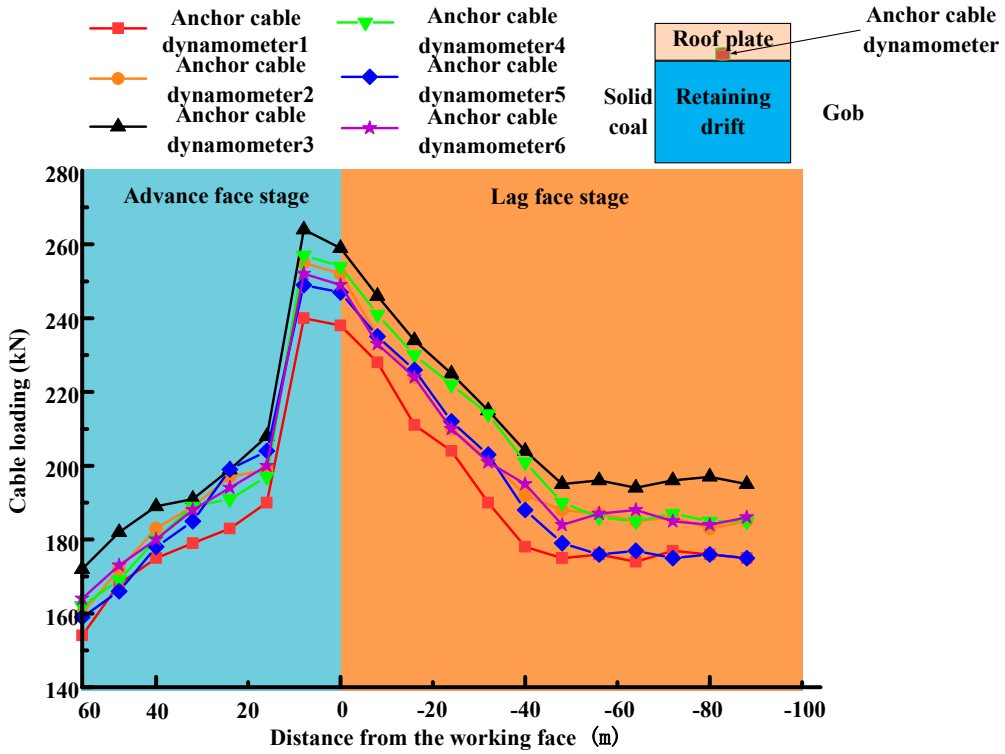

Figure 12. Monitoring curve of the anchor cable dynamometer.

(2) Roof separation instruments

The monitoring curves of the roof separation instruments are shown in Figure 13. Under the cutting heights of 7.8 m and 8 m and the original plan's cutting height of 9.35 m, the separation amounts during the monitoring period show little difference, and the separation amounts are negligible, with some instances recording a separation amount of zero. The monitoring results indicate that the current cutting strategy, which ensures the fracture of the basic roof's four gray layers, effectively suppresses roof deformation. The separation amounts under the three cutting heights are similar, demonstrating that a cutting height of 7.8 m is sufficient to ensure the smooth collapse of the basic roof's four gray layers.

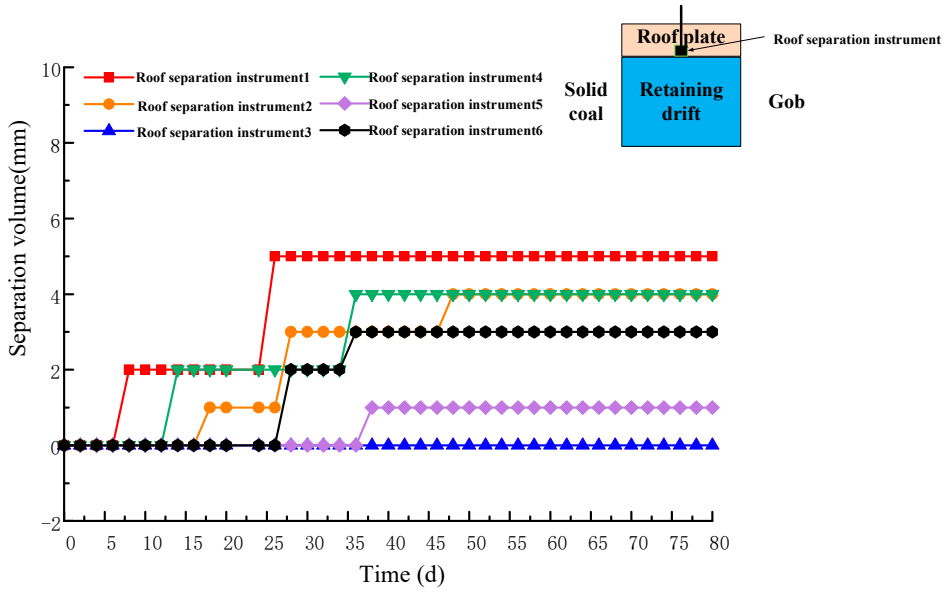

Figure 13. Monitoring curve of the roof separation instrument.

5.3. Analysis of Roof Cutting Effects

The collapse effect of the goaf behind the support was observed through a viewing hole. The opening of the viewing hole is located 20 m behind the fully mechanized support, with an angle of 50° to the direction of mining, inclined backward. The bottom of the hole is situated within the four gray layers of the old goaf behind the support. The observation results are shown in Figure 14. The view of the goaf at the working face indicates that the four gray layers of the goaf roof have collapsed.

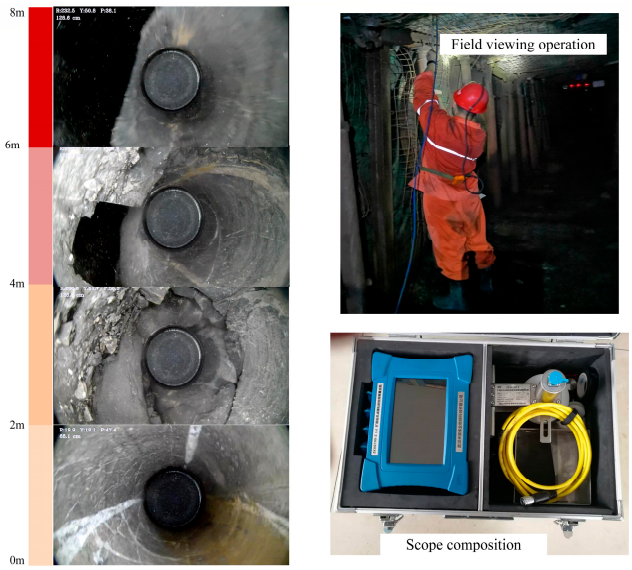

Figure 14. Backfall effect observation.

5.4. Comparative Analysis of Benefits Before and After Roof Cutting Height Adjustment

Through field research at the Qiuji Coal Mine, it was found that the construction cost for cutting holes is 150 yuan/m. By adjusting the cutting height from the original 9.35 m to an optimized 7.8 m, the drilling depth per hole is reduced from 9.5 m to 8 m (Table 6). For every 100 m of cutting holes, a savings of 22,500 yuan in construction costs can be achieved. Taking the 12 1103 working face as an example, with a length of 946 m, the total savings in construction costs would amount to 212,900 yuan, along

with a 15% increase in construction efficiency. Beyond direct drilling costs, this optimized cutting height of 7.8 m generates significant additional economic benefits. Analysis of historical data shows a 30% reduction in tunnel maintenance costs, saving approximately 180,000 yuan annually. The enhanced roof stability simultaneously reduces production interruptions, increasing operational availability by 8% and contributing 250,000 yuan annually through improved production continuity. Therefore, through a detailed analysis of the cutting height, significant improvements in construction efficiency and production cost savings can be realized.

Table 6. Cost comparison of cutting heights.

Parameter	Original (9.35 m)	Optimized (7.8 m)	Reduction
Drilling depth per hole	9.5 m	8.0 m	15.8%
Cost per meter	150 yuan/m	127.5 yuan/m	15%
Annual maintenance cost	600,000 yuan	420,000 yuan	180,000 yuan

6. Discussion

The cutting height has always been a key parameter in the design of gob-side entry retention. This paper constructs a lateral roof mechanical model of the mined-out area and presents cutting height calculation formulas under two scenarios, analyzing the deformation mechanisms of the roof under different conditions of gob material expansion. Additionally, the proposed method of analyzing and calculating the cutting height through the lateral roof of the mined-out area represents a novel approach to the existing techniques in gob-side entry retention. A more detailed study of the cutting height is highly important for ensuring safety in coal mining operations.

In previous research, cutting height calculations for gob-side entry retention were based on the height of gob material expansion. However, the expansion characteristics of rocks are influenced by various factors, including the physical and mechanical properties of the rock, the degree of fragmentation, and the size of the fragments. The complexity and variability of these factors can lead to inaccuracies in measuring and predicting the expansion coefficient, often resulting in cutting heights that are either too large or too small in practical operations, thereby impacting safety in coal mining.

Nevertheless, calculating the cutting height via a lateral roof mechanical model for a mined-out area requires further investigation, including the supporting effects below the cut seam after beam bending, the uneven accumulation of gob material after collapse, and the actual effects of onsite cutting blasting. This study analyzes only one coal seam working face, so its geological applicability needs to be further validated in practice. The model developed in this study has several limitations that warrant consideration. First, the lateral mechanical model assumes homogeneous material properties within each layer, whereas real geological formations exhibit heterogeneity and anisotropy. Second, dynamic effects during roof collapse and time-dependent behaviors are not fully captured in the current model. Third, the influence of water and gas pressure on roof stability is not incorporated into the calculation formulas.

Future research should focus on comparing our findings with alternative numerical approaches such as discrete element methods (DEMs), finite element methods (FEMs), and boundary element methods (BEMs) to evaluate the accuracy and applicability of different modeling techniques. Additionally, three-dimensional models that account for spatial variations in geological conditions should be developed to provide more comprehensive predictions. Machine learning algorithms could also be integrated with numerical simulations to improve prediction accuracy by incorporating real-time monitoring data from mining operations. In the future, more diversified simulation analysis software may be

able to calculate cutting heights suitable for different working conditions more accurately, thereby ensuring safety in coal mining operations.

7. Conclusions

This study developed a lateral mechanical model for goaf roofs based on collapse characteristics and composite beam theory, while considering gangue bulking effects. Through theoretical analysis, numerical simulation, and field experiments, we derived an optimal cutting height formula and verified its effectiveness for improving roof stability and construction efficiency. The main findings are summarized as follows:

(1) On the basis of the collapse characteristics of a goaf roof and the theory of composite beams, a lateral mechanical model of a goaf roof for a working face was constructed while considering the bulking of gangue in the goaf. By combining the theory of ultimate tensile stress and the Maxwell model, a formula for calculating the optimal cutting height of a composite hard roof was derived. Considering the geological conditions of the 12 1103 working face at the Qiuji Coal Mine, the optimal cutting height was determined to be 7.8 m.

(2) UDEC 7.0 was used to simulate roof subsidence under different cutting heights, and an analysis of the numerical simulation results indicated that cutting and pressure relief had a significant effect on the stability of the composite hard roof and the suppression of floor heave in the goaf. An analysis of the roof collapse conditions, vertical displacement, and stress distribution in the roadway revealed that a cutting height of 7.8 m yields the best results for roadway stability. Further increases in the cutting height did not significantly improve the roadway stability.

(3) Experiments were conducted at the 12 1103 working face with three different cutting heights: 7.8 m, 8 m, and an original height of 9.35 m. A comparative analysis of the monitoring curves from the roof anchor force gauges and the roof separation meters in the experimental section revealed that the forces acting on the roof anchors and the separation amounts were similar for all three cutting heights. The cutting height of 7.8 m ensures that the four gray layers of the basic roof collapse smoothly under their own weight. Field observations from drilling also indicated that the four gray layers of the goaf roof essentially collapsed. On the basis of the cost survey of cutting hole construction, adjusting the cutting height to 7.8 m for the 12 1103 working face could save approximately 156,000 yuan compared with the original plan while improving the construction efficiency by 15%.

Author Contributions: Conceptualization, J.W. and D.B.; methodology, Y.Z. (Yong Zhang) and Y.Z. (Yuxuan Zhang); software, J.W.; validation, P.L., Q.C. and Y.Z. (Yong Zhang); formal analysis, Q.Z.; investigation, D.B.; resources, Y.Z. (Yong Zhang); data curation, J.W.; writing—original draft preparation, J.W.; writing—review and editing, J.W.; visualization, Q.Z.; supervision, Q.Z.; project administration, J.W.; funding acquisition, J.W. All authors have read and agreed to the published version of the manuscript.

Funding: This research was funded by the National Natural Science Foundation of China (No. 41772299) and the Natural Science Foundation of Shandong Province, China (No. ZR2023ME165).

Data Availability Statement: The data presented in this study are available on request from the corresponding author. The data are not publicly available due to privacy and legal concerns.

Conflicts of Interest: Authors Dongdong Bai, Yon Zhang, Peiyue Liu, Qingyu Chen and Yuxuan Zhang were employed by the company Shandong Qiuji Co., Ltd. The remaining authors declare that the research was conducted in the absence of any commercial or financial relationships that could be construed as a potential conflict of interest.

References

1. Li, X.G.; Zhang, X.Y.; Zhang, Y.; Tu, M.; Gao, Y.G.; Bu, Q.W.; Zhao, X.Y. Study on Pressure Control and Recovery Rate of Initial Mining in Super Thick Coal Seam with Hard Roof. *Mining Res. Dev.* **2022**, *42*, 20–28. [CrossRef]
2. Xie, H.P. Research Progress on Mechanics and Mining Theory of Deep Rock Mass. *J. China Coal Soc.* **2019**, *44*, 1283–1305.
3. Li, A.L.; Wang, S.; Gou, R.T.; Li, Z.C.; Huang, W. Research on Front Cutting Pressure Relief Technology of Hard Roof Working Face Support. *Mining Res. Dev.* **2024**, *44*, 85–91. [CrossRef]
4. Wang, W.; Zheng, S.T.; Li, W.J.; Du, B.T.; Luo, A.K. Water Damage Analysis and Control Technology of Double Limestone on Top and Bottom of Huangbei Coalfield. *Coal Mine Saf.* **2020**, *51*, 93–96. [CrossRef]
5. Yan, S.; Liu, T.; Bai, J.; Wu, W. Key Parameters of Gob-Side Entry Retaining in a Gassy and Thin Coal Seam with Hard Roof. *Processes* **2018**, *6*, 51. [CrossRef]
6. Sun, J. Study on Failure Characteristics and Water Inrush Mechanism of Inclined Coal Seam Floor. Ph.D. Thesis, China University of Mining and Technology, Xuzhou, China, 2011.
7. Wang, J.M.; Ge, J.D.; Wu, Y.H. Mechanism on Progressive Intrusion of Pressure Water under Coal Seams into Protective Aquiclude and Its Application in Prediction of Water Inrush. *J. Coal Sci. Eng.* **1996**, *2*, 9–15.
8. He, M.C.; Song, Z.Q.; Wang, A.; Yang, H.H.; Qi, H.G.; Guo, Z.B. Longwall Mining Short-Wall Beam Theory and Its 110 Construction Method: The Third Mining Science and Technology Reform. *Coal Sci. Technol.* **2017**, *1*, 1–13. [CrossRef]
9. Cui, J.B. Technical Research on Caving Problems of Hard Roof by Cutting Off Roof Blasting along Goaf. Master's Thesis, Shandong University of Science and Technology, Qingdao, China, 2024.
10. Su, X.S.; Wei, H.Y.; Su, Y. Research on Key Technologies of Roof Cutting and Roadway Retention under Complex Roof Conditions. *Coal Sci. Technol.* **2019**, *47*, 70–77. [CrossRef]
11. Wang, F.R.; Wu, C.L.; Yao, Q.L. Instability Mechanism and Control Method of Surrounding Rock of Water-Rich Roadway Roof. *Minerals* **2022**, *12*, 1587. [CrossRef]
12. Tian, C.; Wang, A.; Liu, Y.; Jia, T. Study on the Migration Law of Overlying Strata of Gob-Side Entry Retaining Formed by Roof Cutting and Pressure Releasing in the Shallow Seam. *Shock Vib.* **2020**, *2020*, 8821160. [CrossRef]
13. Wang, H.; Chen, Z.; Wang, X.L.; Zhang, S. Determination and Application of Key Parameters of Hard Rock Roof Cutting and Roadway Retention. *Saf. Coal Mines* **2023**, *54*, 153–162. [CrossRef]
14. Liu, Z.; Wang, J.; Zhang, C. UDEC-Based Analysis of Roof Fracture Evolution in Deep Coal Mines. *Rock Mech. Rock Eng.* **2021**, *54*, 4567–4582. [CrossRef]
15. Chen, L.; Xu, H.; Zhou, W. AI-Optimized Top-Cutting Parameters for Hard Roof Control Using Genetic Algorithms. *Autom. Constr.* **2023**, *145*, 104632. [CrossRef]
16. Shi, W.P.; Li, Z.Y.; Liu, C.T.; Lv, Y.W.; Zhang, H.R.; Yang, T. Research on Optimization of Key Parameters for Cutting Roadway with Thick Hard Roof in Inclined Coal Seam. *Coal Sci. Technol.* **2024**, *52*, 11–24.
17. Zhang, F.; Wang, G.; Li, S. Field Validation of Numerical Models for Roof Cutting in Thick Coal Seams. *J. Min. Saf. Eng.* **2019**, *36*, 1120–1128. [CrossRef]
18. Yang, X.; Mao, W.; Wang, E.; Sun, Y.; Wang, J.; He, M. Mechanism and Control Methods of Roof Deformations in Gob-Side Entry Retention by Roof Cutting under Medium-Thick Coal Seams. *Geotech. Geol. Eng.* **2020**, *38*, 265–282. [CrossRef]
19. Gao, Y.B.; Yang, J.; Wang, Q.; Wang, Y.J.; He, M.C. Mechanism of Pre-Cracking and Roof Cutting in Self-Formed Roadway without Coal Pillar and Its Influence on Ore Pressure Development. *J. China Coal Soc.* **2019**, *44*, 3349–3359.
20. Ma, X.G.; He, M.C.; Li, Z.; Liu, Y.X.; Yu, G.Y.; Du, H.R. Research on Key Parameters of Roof Blasting Design of Self-Forming Roadway with Composite Roof without Coal Pillar. *J. China Univ. Min. Technol.* **2019**, *48*, 236–277. [CrossRef]
21. Ma, G.X. Study on Rock Crushing and Swelling Law of Deep and Thick Coal Seam under Roof Cutting and Unloading. *Coal Eng.* **2019**, *51*, 118–121.
22. Ma, Q.; Zhang, Y.; Li, Z.; Song, G.; Zheng, Y. The Roadway Layout and Control Technology of Pillar-Free Mining of Soft Coal Seams in High Gassy Mines. *Processes* **2022**, *10*, 1784. [CrossRef]
23. Terzaghi, K.; Peck, R.B.; Mesri, G. *Soil Mechanics in Engineering Practice*, 3rd ed.; Wiley: New York, NY, USA, 1996.
24. Ma, L.; Xing, L.; Liu, C.; Cui, T.; Qiao, X.; Miao, W.; Kong, P. Research on the Instability Mechanism and Control Technology of Gob-Side Entry in Deep Mines with Soft Rock. *Buildings* **2025**, *15*, 19. [CrossRef]
25. Findley, W.N.; Lai, J.S.; Onaran, K. *Creep and Relaxation of Nonlinear Viscoelastic Materials*; Dover: Mineola, NY, USA, 1976.

Disclaimer/Publisher's Note: The statements, opinions and data contained in all publications are solely those of the individual author(s) and contributor(s) and not of MDPI and/or the editor(s). MDPI and/or the editor(s) disclaim responsibility for any injury to people or property resulting from any ideas, methods, instructions or products referred to in the content.